antioxidants

MDPI

Article

Chlorogenic Acid Attenuates Aflatoxin B1-Induced HepG2 Cell Injury by Modulating Oxidative Stress, Mitochondrial Function, and Ferroptosis-Associated Responses

Dahai Jiang [1,2,3,4], Manqi Yang [1,2,3], Huiliang Gan [1], Liming Lu [1,2,3,*] and Jianchun Jiang [1,2,3,5]

[1] College of Chemical Engineering, Huaqiao University, Xiamen 361021, China
[2] Academy of Advanced Carbon Conversion Technology, Huaqiao University, Xiamen 361021, China
[3] Fujian Provincial Key Laboratory of Biomass Low-Carbon Conversion, Huaqiao University, Xiamen 361021, China
[4] Hangzhou Institute of Medicine, Chinese Academy of Sciences, Hangzhou 310018, China
[5] Institute of Chemical Industry of Forest Products, Chinese Academy of Forestry, Nanjing 210042, China
* Correspondence: lulm@hqu.edu.cn

Abstract

Aflatoxin B1 (AFB1) is a hepatotoxic mycotoxin that induces hepatocellular injury through oxidative stress, mitochondrial dysfunction, and other cellular stress responses. Chlorogenic acid (CGA), a dietary phenolic acid with antioxidant and hepatoprotective properties, may attenuate AFB1-associated cellular injury; however, its effects on iron- and lipid-peroxidation-associated responses remain incompletely understood. In this study, human HepG2 cells were used to establish an in vitro AFB1-induced injury model. Cell viability, cell morphology, Hoechst 33342/PI staining, LDH release, extracellular ALT/AST activities, antioxidant status, ROS accumulation, mitochondrial membrane potential, intracellular Fe^{2+} and total iron levels, and the mRNA expression of selected apoptosis- and ferroptosis-associated genes were evaluated. AFB1 reduced HepG2 cell viability in a concentration-dependent manner, and 16 μM AFB1 was selected for subsequent experiments. CGA concentrations of 12.5–50 μM retained cell viability above 90% in the CGA-alone screening assay, although modest statistically significant reductions were observed at 25 and 50 μM. CGA pretreatment improved AFB1-impaired cell viability and morphology, decreased LDH release and extracellular ALT/AST activities, increased GSH content and T-SOD activity, and reduced ROS and lipid-peroxidation-associated indicators. CGA also partially modulated AFB1-associated changes in *BAX*, *BCL-2*, and *Caspase-3* mRNA expression and attenuated the JC-1 fluorescence changes associated with mitochondrial membrane potential. In addition, CGA reduced the measured intracellular Fe^{2+} and total iron levels and modulated the transcript abundance of ferroptosis-associated genes, including *ACSL4*, *P53*, *TXNIP*, *Trx-1*, and *GPX4*. These findings indicate that the protective effects of CGA are associated with improvements in cellular redox status, mitochondrial function, and iron- and lipid-peroxidation-related responses.

Keywords: chlorogenic acid; aflatoxin B1; HepG2; oxidative stress; ferroptosis-associated responses

Check for updates

Academic Editor: Carla Susana Correia Pereira

Received: 22 September 2026
Revised: 5 November 2026
Accepted: 15 November 2026
Published: 17 November 2026

Copyright: © 2026 by the authors. Licensee MDPI, Basel, Switzerland. This article is an open access article distributed under the terms and conditions of the Creative Commons Attribution (CC BY) license.

1. Introduction

Aflatoxin B1 (AFB1), a difuranocoumarin secondary metabolite mainly produced by *Aspergillus flavus* and *Aspergillus parasiticus*, remains one of the most concerning naturally occurring contaminants in food and feed systems. It frequently occurs in cereals, peanuts,

tree nuts, oil crops, and animal-derived products through contaminated feed, and its chemical stability makes complete elimination difficult during routine processing, storage, and cooking. Repeated dietary exposure makes AFB1 an important toxicological and food-safety concern. The liver is a primary target organ for AFB1 biotransformation and toxicity; therefore, clarifying AFB1-induced hepatocellular injury and identifying protective agents are important for risk control and nutritional intervention [1–5]. AFB1 hepatotoxicity is associated with metabolic activation, oxidative damage, mitochondrial dysfunction, inflammatory signaling, and multiple cellular stress responses. Hepatic cytochrome P450 enzymes can convert AFB1 to reactive epoxide metabolites that form DNA and protein adducts. In parallel, AFB1 exposure can disturb mitochondrial function, enhance ROS generation, weaken antioxidant defenses, and promote lipid peroxidation. These processes indicate that AFB1-induced liver injury is multifactorial rather than attributable to a single pathway [1–4].

Natural bioactive compounds have received increasing attention as complementary strategies to mitigate mycotoxin-induced liver injury because many of them simultaneously regulate oxidative stress, inflammation, mitochondrial homeostasis and lipid metabolism. Chlorogenic acid (CGA), an ester of caffeic acid and quinic acid, is abundant in coffee, tea, fruits, vegetables and several medicinal plants. CGA has been reported to display antioxidant, anti-inflammatory, metabolic regulatory and hepatoprotective properties. Recent evidence indicates that CGA alleviates AFB1-induced hepatotoxicity in mice by modulating oxidative stress and inflammation [1], and another study reported that CGA improved mitochondrial function, activated Nrf2/HO-1 signaling and inhibited noncanonical NF-κB signaling during AFB1 exposure [2]. These findings support CGA as a promising natural compound for hepatoprotection, but its regulatory influence on ferroptosis-related events requires deeper investigation. Comparable antioxidant protection against AFB1 has also been reported for alpha-lipoic acid/coenzyme Q10 and Spirulina-based interventions [6,7].

Ferroptosis is an iron-dependent form of regulated cell death associated with excessive lipid-peroxide accumulation. It is commonly characterized by disturbances in iron homeostasis, glutathione (GSH) depletion, impaired glutathione peroxidase 4 (GPX4)-dependent lipid-peroxide control, and oxidation of polyunsaturated-fatty-acid-containing phospholipids [8–11]. The System Xc−/GSH/GPX4 axis contributes to cellular protection: SLC7A11-mediated cystine uptake supports GSH synthesis, while GPX4 reduces lipid hydroperoxides [12–15]. Conversely, acyl-CoA synthetase long-chain family member 4 (ACSL4) promotes the incorporation of polyunsaturated fatty acids into membrane phospholipids and can increase their susceptibility to peroxidation [16,17]. Dysregulation of iron handling, lipid metabolism, and antioxidant defenses can therefore contribute to ferroptosis susceptibility [18–23]. Experimental suppression of GPX4 and SLC7A11 has also been shown to induce ferroptotic death in hepatocellular carcinoma cells [24]. However, changes in individual biochemical indicators or transcript abundance alone do not establish ferroptotic cell death. The liver is particularly relevant to ferroptosis research because of its central roles in iron storage, xenobiotic metabolism, lipid turnover, and antioxidant defense [8–10,12]. Mitochondrial function and intracellular labile iron availability are also closely linked to ferroptosis regulation [25,26].

Evidence linking AFB1 toxicity with ferroptosis-associated responses has expanded in recent years. Hesperetin was reported to alleviate AFB1-induced liver toxicity by modulating lipid peroxidation and ferritin autophagy [27], while baicalin protected against AFB1-induced hepatocyte injury through a P53-related ferroptosis pathway [28]. These studies suggest that AFB1 exposure may be accompanied by disturbances in iron handling and lipid-peroxidation homeostasis. However, cellular responses may differ according to cell type, exposure intensity, and intervention strategy. It is therefore relevant to examine

whether CGA modulates AFB1-associated changes in intracellular iron, lipid-peroxidation indicators, and the expression of selected genes associated with ferroptosis in a defined hepatocyte-derived cell model.

Studies of natural products have also examined iron- and lipid-peroxidation-related responses in liver injury models. Salvianolic acid B, quercetin, theaflavins, and sesamin have been reported to affect different regulators associated with iron handling, antioxidant defense, or ferroptosis-related processes [29–32]. These studies provide a rationale for examining iron accumulation, lipid-peroxidation indicators, and selected ferroptosis-associated transcripts in the context of CGA treatment. In the present study, *ACSL4*, *P53*, *TXNIP*, *Trx-1*, and *GPX4* were evaluated as molecular indicators related to lipid metabolism and cellular redox regulation. Because these targets are regulated at multiple molecular levels, transcript measurements are considered complementary molecular observations rather than direct evidence of protein abundance, enzymatic activity, or ferroptotic cell death. Broader reviews of CGA describe its antioxidant and metabolic actions and therapeutic potential [33,34]. Additional studies and reviews have linked natural compounds to ferroptosis-related regulation in diverse liver-injury models, including effects involving SLC7A11/GPX4 signaling, iron handling, and lipid peroxidation [35–43].

Therefore, the present study established an AFB1-induced HepG2 cell injury model and evaluated the effects of CGA using biochemical, morphological, mitochondrial, and molecular endpoints. We assessed cell viability, cell morphology, Hoechst 33342/PI staining, LDH release, extracellular ALT/AST activities, GSH, T-SOD, ROS, MDA, LPO, mitochondrial membrane potential, intracellular Fe^{2+} and total iron, and the mRNA expression of selected apoptosis- and ferroptosis-associated genes. The study aimed to determine whether CGA attenuates AFB1-associated cellular injury and modulates oxidative, mitochondrial, iron-related, and lipid-peroxidation responses. This study provides an experimental framework for understanding CGA-mediated protection against AFB1-induced hepatotoxicity.

2. Materials and Methods

2.1. Reagents

AFB1 (Cat. No. B24051), CGA (Cat. No. B20782), and N-acetyl-L-cysteine (NAC; Cat. No. S20137) were obtained from Shanghai Yuanye Bio-Technology Co., Ltd. (Shanghai, China). DMSO (Cat. No. D8371), DMEM (Cat. No. 11995), FBS (Cat. No. S9030), penicillin–streptomycin solution (Cat. No. P1400), and PBS (Cat. No. P1020) were purchased from Beijing Solarbio Science & Technology Co., Ltd. (Beijing, China). AFB1, CGA, and NAC were dissolved in DMSO to prepare stock solutions and subsequently diluted with complete culture medium to the required working concentrations. Cell viability was assessed using a Cell CCK-8 (Cat. No. CA1210), intracellular reactive oxygen species were detected using a ROS Assay Kit (Cat. No. CA1410), cell viability and membrane integrity were evaluated using a Hoechst 33342/PI Double Stain Kit (Cat. No. CA1120), and mitochondrial membrane potential was determined using a JC-1 Mitochondrial Membrane Potential Assay Kit (Cat. No. M8650), all obtained from Solarbio. Intracellular total iron and Fe^{2+} levels were measured using a Cell Iron Content Assay Kit (Cat. No. BC5315) and a Ferrous Ion Content Assay Kit (Cat. No. BC5415), respectively. GSH, T-SOD, MDA, and LPO were determined using the corresponding assay kits (Cat. No. BC1175, BC0175, BC0025, and BC5245, respectively; Solarbio). ALT, AST, and LDH were measured using the corresponding assay kits (Cat. No. BC1555, BC1565, and M1030, respectively; Solarbio). Total RNA was extracted using TriQuick Reagent (Cat. No. R1100; Solarbio). cDNA was synthesized using the PrimeScript™ RT reagent Kit with gDNA Eraser (Cat. No. RR047A; Takara, Beijing, China), and quantitative real-time PCR was performed using

TB Green® Premix Ex Taq™ II (Tli RNaseH Plus) (Cat. No. RR820A; Takara) according to the manufacturers' instructions.

2.2. Cell Culture

HepG2 cells were obtained from the American Type Culture Collection (ATCC, HB-8065). HepG2 cells were cultured in high-glucose DMEM supplemented with 10% fetal bovine serum and 1% penicillin–streptomycin. Cultures were maintained at 37 °C in a humidified atmosphere containing 5% CO_2. Cells in the logarithmic growth phase were used for all experiments, and culture medium and treatment solutions were prepared under the same incubation conditions.

2.3. Experimental Design

Dose–response experiments were first performed to select the AFB1 challenge concentration and the CGA concentration range for the protection experiments. HepG2 cells were exposed for 24 h to AFB1 at 0, 2, 4, 8, 16, or 32 μM, or to CGA at 0, 12.5, 25, 50, 100, or 200 μM, after which cell viability was assessed using the CCK-8 assay. On the basis of these screening results, 16 μM AFB1 was selected for the cell-injury model, and 12.5, 25, and 50 μM CGA were selected for the protection experiments. For the intervention protocol, cells were pretreated with CGA for 6 h and then exposed to 16 μM AFB1 for 24 h. Importantly, the CGA-containing culture medium was not removed or replaced before AFB1 addition; instead, AFB1 was added directly to the existing medium. NAC (10 μM) was included as a positive antioxidant reference. The present study used a pretreatment design; a post-treatment intervention was not examined. All comparisons and downstream measurements were performed using these predefined treatment conditions.

2.4. Cell Viability and Morphology

Cell viability was evaluated using the CCK-8 assay. Before experiments, the cell suspension was adjusted to a seeding concentration of 1×10^5 cells/mL. At the end of the indicated treatment period, CCK-8 reagent was added to each well and the cells were incubated according to the reagent protocol. Absorbance was then recorded with a microplate reader and used to estimate relative cell viability. In parallel, cellular morphology was examined by inverted microscopy. Changes in cell shape, attachment, and overall monolayer appearance were documented from representative microscopic fields.

2.5. Hoechst 33342/PI Staining

Following treatment, cells were washed with PBS and incubated with Hoechst 33342 and PI in staining buffer at 4 °C in the dark, according to the assay instructions. Fluorescence images were acquired using an inverted fluorescence microscope (Dmil LED Fluo, Leica, Wetzlar, Germany). Hoechst 33342 staining was used to visualize cell nuclei, whereas PI uptake was used as an indicator of loss of plasma-membrane integrity. The resulting images were evaluated qualitatively to compare the appearance and distribution of membrane-compromised cells among treatment groups.

2.6. Biochemical Assays

Culture supernatants were collected after treatment for determination of LDH release and ALT and AST activities. Intracellular redox status was assessed by measuring T-SOD activity and GSH content, whereas MDA and LPO were measured as indicators of lipid-peroxidation-associated changes. Intracellular ROS generation was detected with the DCFH-DA fluorescent probe and quantified using a fluorescence microplate reader. Mitochondrial membrane potential was evaluated qualitatively by JC-1 staining. Intracellular Fe^{2+} and

total iron contents were determined colorimetrically with the corresponding assay kits. According to the units presented in the figures, T-SOD activity and MDA content were normalized to protein content; GSH and LPO were reported as assay-based concentrations (μg/mL and nmol/mL, respectively); ROS was expressed as relative fluorescence (% of control); Fe^{2+} and total iron were expressed per 10^6 cells; and LDH, ALT, and AST were reported as activities measured in culture supernatants. These endpoints were therefore not all normalized using a common protein- or cell-number-based reference and should be interpreted according to their respective assay outputs. Each assay was conducted according to the manufacturer's protocol and the treatment conditions described in Section 2.3.

2.7. Quantitative Real-Time PCR

Total RNA was isolated from treated cells and reverse-transcribed into cDNA using the designated reverse-transcription reagents. Quantitative real-time PCR was performed with TB Green master mix. GAPDH served as the internal reference gene, and relative mRNA expression was calculated using the $2^{-\Delta Ct}$ method. Primer sequences for the analyzed genes are provided in Table 1. The qPCR results are therefore interpreted as changes in transcript abundance and not as direct evidence of corresponding protein abundance or enzymatic activity.

Table 1. Primer sequences used for qRT-PCR analysis.

Gene	Accession No.	Primer	Sequence (5′-3′)
GPX4	NM_002085.5	GPX4-F GPX4-R	ACAAGAACGGCTGCGTGGTGAA GCCACACACTTGTGGAGCTAGA
ACSL4	NM_004458.3	ACSL4-F ACSL4-R	CTCCTCAGTCGGCAGCCAAG GCTCATCCGTCAGGACCTTC
P53	NM_000546.6	P53-F P53-R	ACGCTTCGAGATGTTCCGAG TTTTATGGCGGGAGGGAGAC
TXNIP	NM_006472.6	TXNIP-F TXNIP-R	CAACTTGCTGCCCGACAAAA TGGGTGGCATGCAAGGTATT
TRX-1	NM_003329.4	Trx-F Trx-R	GTGAAGCAGATCGAGAGCAAG CGTGGCTGAGAAGTCAACTACTA
GAPDH	NM_002046.7	GAPDH-F GAPDH-R	ACTGTCAAGGCTGAGAACGG GCCTTCTCCATGGTGGTGAA
BCL-2	NM_000633.3	BCL-2-F BCL-2-R	GCCCTGTGGATGACTGAGTA AAATCAAACAGAGGCCGCAT
BAX	NM_001291428.2	BAX-F BAX-R	GAACCATCATGGGCTGGACA GAGACAGGGACATCAGTCGC
CASPASE-3	NM_004346.4	CASPASE-3-F CASPASE-3-R	GCCCACCACTGAAAGAGTGA TTCACTTCCTGCCCACAGAC

2.8. Statistical Analysis

Data are expressed as the mean ± SD. Differences among groups were evaluated by one-way analysis of variance followed by multiple-comparison testing. A value of $p < 0.05$ was considered statistically significant. Statistical interpretation was based on comparisons among the prespecified experimental groups for each endpoint—* $p < 0.05$; ** $p < 0.01$; *** $p < 0.001$.

3. Results

3.1. Dose Selection and Cytoprotective Effects of CGA

AFB1 exposure reduced HepG2 cell viability in a concentration-dependent manner (Figure 1A). At 32 μM, cell viability was approximately 56% of the control level, whereas 16 μM produced substantial but incomplete cytotoxicity. The 16 μM concentration was selected for subsequent experiments because it produced a measurable injury response while retaining a viable cell population for evaluating the effects of CGA.

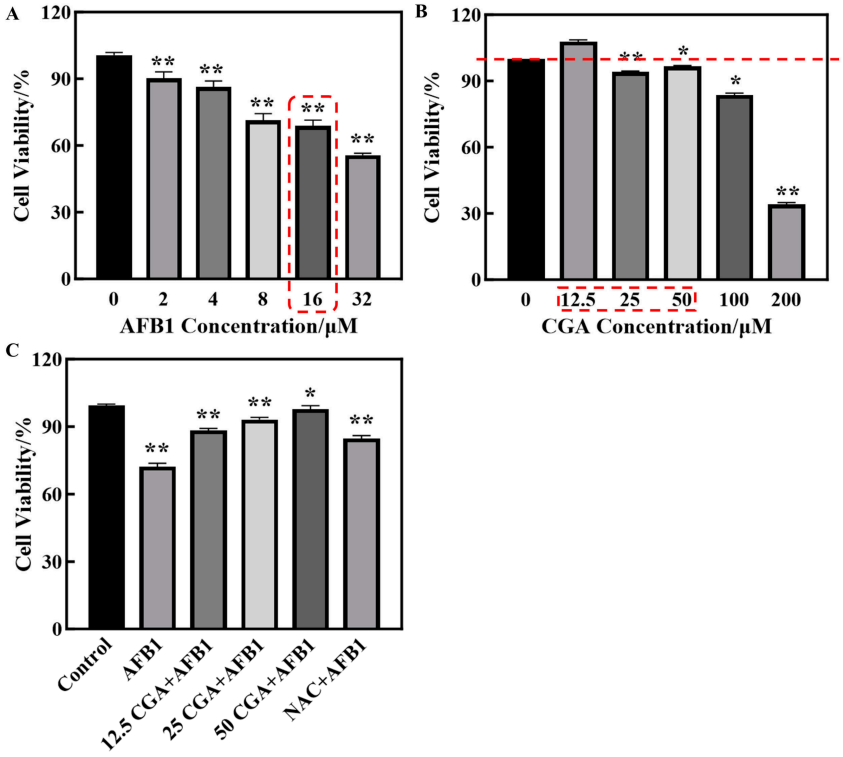


Figure 1. Effects of AFB1 and CGA on HepG2 cell viability. (**A**) Cell viability after 24 h exposure to the indicated AFB1 concentrations (0–32 μM). (**B**) Cell viability after 24 h exposure to CGA alone (0–200 μM). (**C**) Cell viability after CGA pretreatment followed by 16 μM AFB1 exposure. NAC, N-acetyl-L-cysteine, was included as a positive antioxidant control. The dashed lines indicate the parameters used in subsequent experiments. * $p < 0.05$; ** $p < 0.01$.

After 24 h of exposure to CGA alone, cell viability remained above 90% at 12.5–50 μM (Figure 1B). Nevertheless, modest statistically significant reductions were observed at 25 and 50 μM compared with the control group, and these concentrations are therefore not described as completely noncytotoxic. Viability declined more markedly at 100 and 200 μM. The concentrations of 12.5, 25, and 50 μM CGA were selected for subsequent protection experiments to examine responses across this concentration range.

CGA pretreatment improved cell viability in AFB1-exposed cells compared with the AFB1-only group (Figure 1C). Among the tested CGA concentrations, 50 μM produced the highest viability in this assay. The NAC-treated group also showed an improvement relative to AFB1 alone. These results indicate that CGA-associated protection was concentration-related within the tested range, although the relative responses to CGA and NAC should be considered endpoint-specific.

3.2. CGA Attenuates AFB1-Induced Cellular Injury

The CCK-8 results were accompanied by changes in cell morphology and fluorescence staining. Control HepG2 cells showed typical epithelial-like morphology, close cell–cell

contact, and firm attachment. AFB1 exposure was associated with cell shrinkage, rounding, reduced intercellular contact, and detachment (Figures 2 and 3). Hoechst 33342/PI staining showed a stronger PI signal after AFB1 exposure, whereas CGA-pretreated groups showed a less pronounced PI signal than the AFB1-only group (Figure 4). These images are presented as qualitative observations; PI uptake indicates compromised plasma-membrane integrity but does not, by itself, identify a specific mode of cell death.

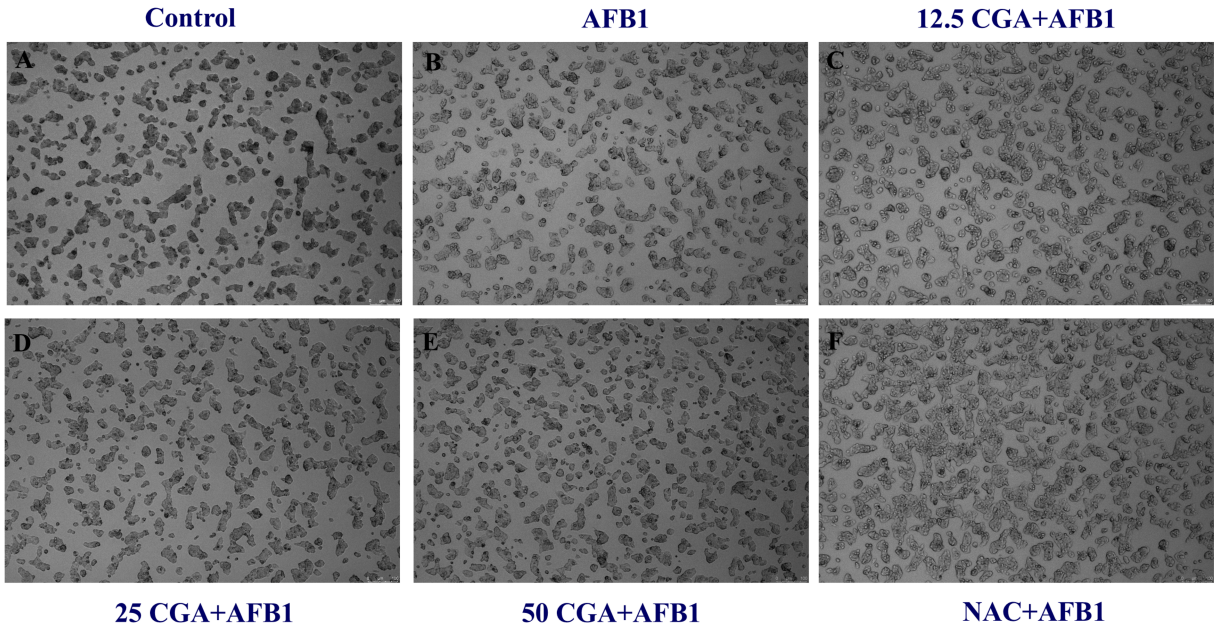


Figure 2. Representative low-magnification bright-field images of HepG2 cell morphology after the indicated treatments: (**A**) Control, (**B**) 16 μM AFB1, (**C**) 12.5 μM CGA + 16 μM AFB1, (**D**) 25 μM CGA + 16 μM AFB1, (**E**) 50 μM CGA + 16 μM AFB1, and (**F**) 10 μM NAC + 16 μM AFB1.

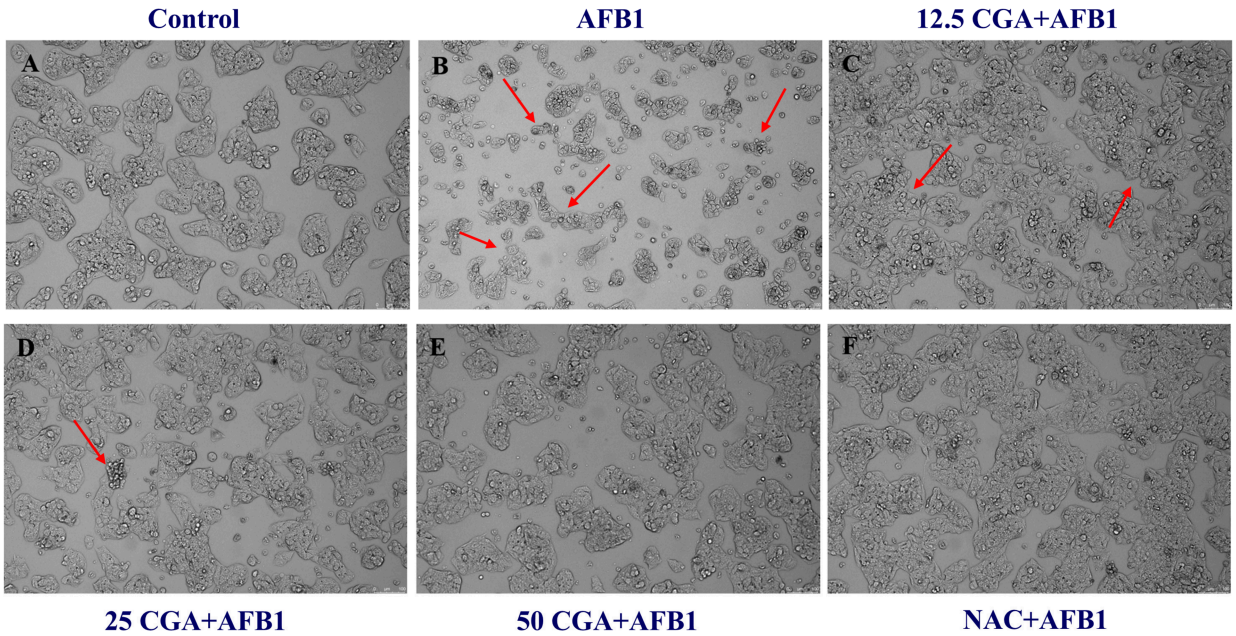


Figure 3. Representative high-magnification bright-field images of HepG2 cells after the indicated treatments: (**A**) Control, (**B**) 16 μM AFB1, (**C**) 12.5 μM CGA + 16 μM AFB1, (**D**) 25 μM CGA + 16 μM AFB1, (**E**) 50 μM CGA + 16 μM AFB1, and (**F**) 10 μM NAC + 16 μM AFB1. The arrows indicate abnormal cells.

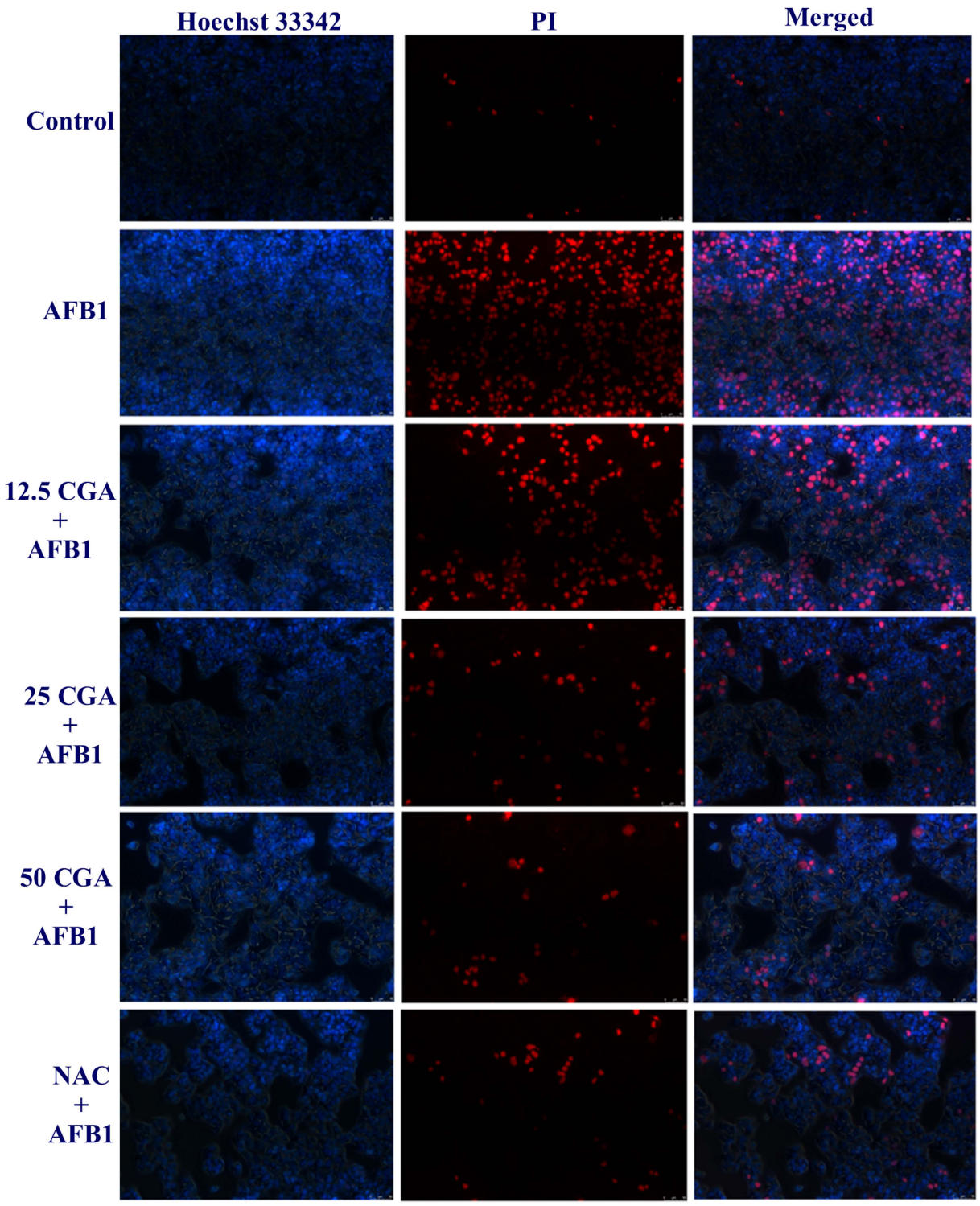


Figure 4. Representative Hoechst 33342/PI fluorescence images of HepG2 cells after the indicated treatments. Rows (top to bottom): Control, 16 μM AFB1, 12.5 μM CGA + 16 μM AFB1, 25 μM CGA + 16 μM AFB1, 50 μM CGA + 16 μM AFB1, and 10 μM NAC + 16 μM AFB1. Columns (left to right): Hoechst 33342 (blue), PI (red), and merged images. PI uptake indicates compromised plasma-membrane integrity. Images are presented as qualitative observations.

3.3. CGA Attenuates AFB1-Associated Membrane Injury

AFB1 exposure increased LDH release and the extracellular activities of AST and ALT in the culture supernatant (Figure 5). CGA pretreatment reduced these measured activities to varying extents across the tested concentrations. LDH release was used as

the principal indicator of membrane damage, whereas AST and ALT activities were considered supplementary indicators of cellular injury. Because extracellular ALT and AST activities in an in vitro HepG2 model are not equivalent to serum transaminase measurements in vivo, these results are interpreted cautiously and alongside the morphological and PI-staining findings.

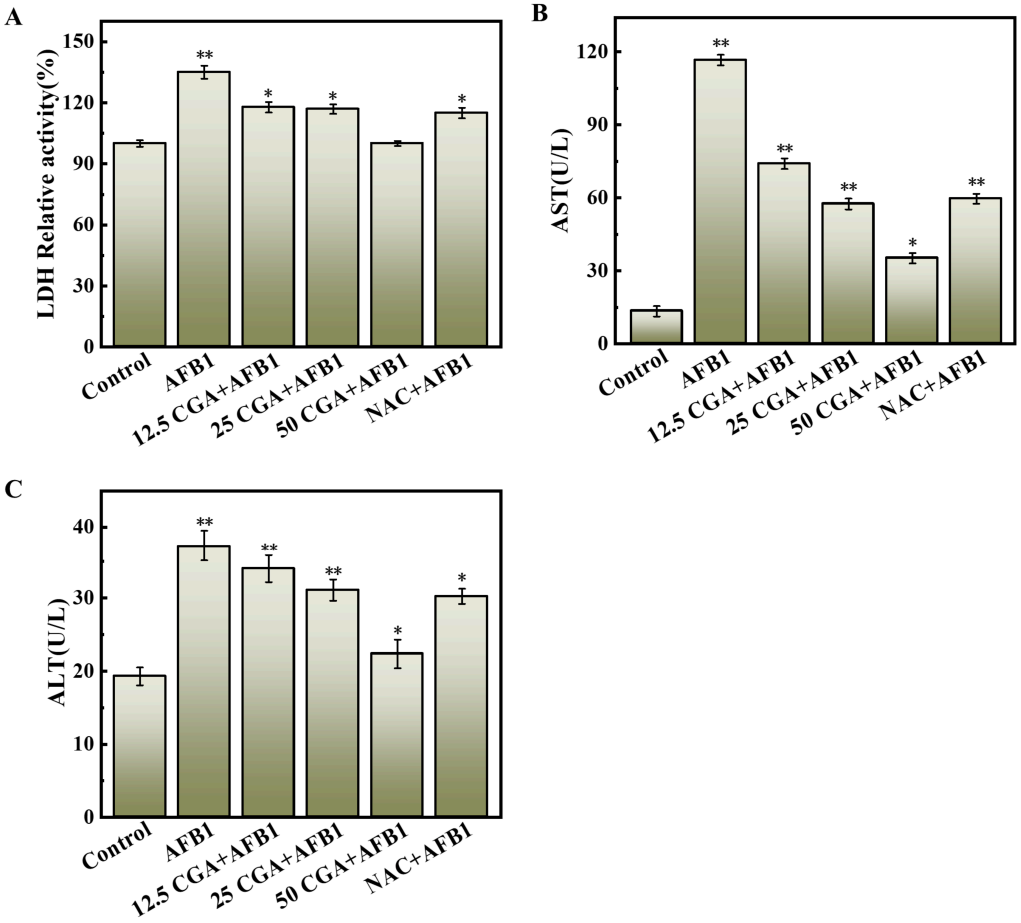


Figure 5. Effects of CGA pretreatment on (**A**) LDH release, (**B**) AST activity, and (**C**) ALT activity in the culture supernatants of AFB1-treated HepG2 cells. The treatment groups were Control, 16 μM AFB1, 12.5 μM CGA + 16 μM AFB1, 25 μM CGA + 16 μM AFB1, 50 μM CGA + 16 μM AFB1, and 10 μM NAC + 16 μM AFB1. * $p < 0.05$; ** $p < 0.01$.

3.4. CGA Modulates Redox Status and Lipid-Peroxidation-Associated Indicators

AFB1 exposure decreased GSH content and T-SOD activity and increased the ROS fluorescence signal, MDA content, and LPO content (Figures 6–8). The increase in MDA was comparatively modest, whereas the relative change in LPO was more pronounced; these measurements represent different assay endpoints and are not directly interchangeable. CGA pretreatment increased GSH and T-SOD measurements and reduced ROS and LPO signals relative to the AFB1-only group. The effects generally became more pronounced across the selected CGA concentration range. At 50 μM, CGA showed numerically favorable responses compared with NAC for several redox endpoints, including GSH, T-SOD, ROS, and LPO.

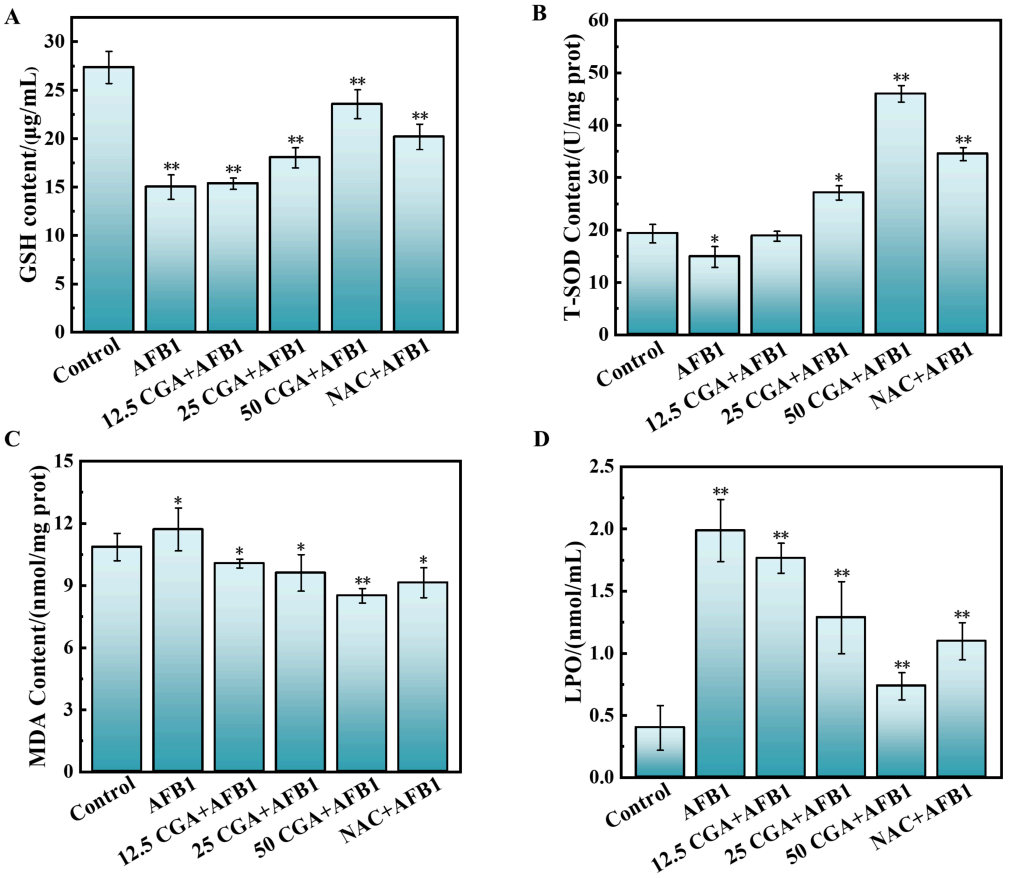


Figure 6. Effects of CGA pretreatment on (**A**) GSH content (μg/mL), (**B**) T-SOD activity (U/mg protein), (**C**) MDA content (nmol/mg protein), and (**D**) LPO content (nmol/mL) in AFB1-treated HepG2 cells. * $p < 0.05$; ** $p < 0.01$.

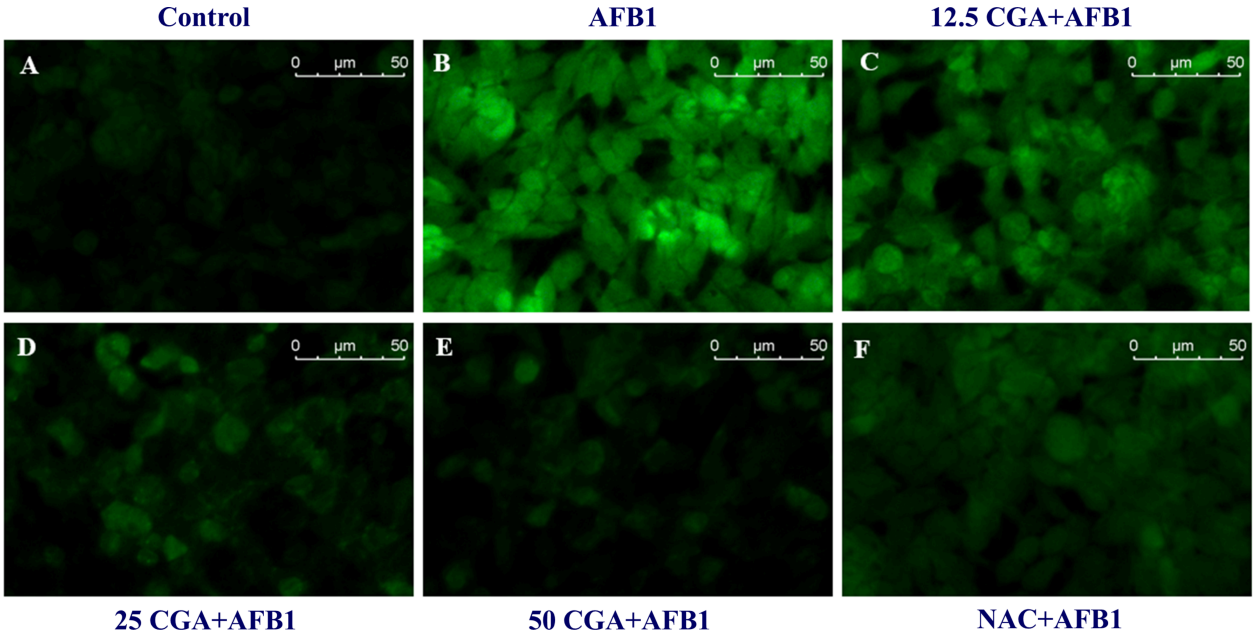


Figure 7. Representative DCFH-DA fluorescence images showing intracellular ROS-associated fluorescence in HepG2 cells after the indicated treatments: (**A**) Control, (**B**) 16 μM AFB1, (**C**) 12.5 μM CGA + 16 μM AFB1, (**D**) 25 μM CGA + 16 μM AFB1, (**E**) 50 μM CGA + 16 μM AFB1, and (**F**) 10 μM NAC + 16 μM AFB1.

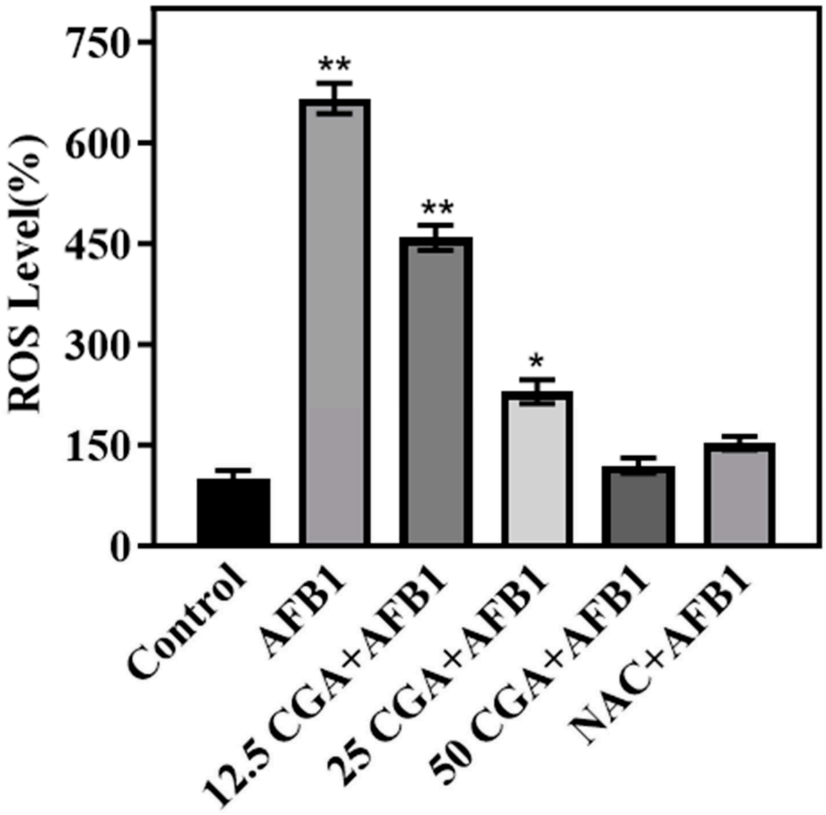


Figure 8. Quantification of the DCFH-DA fluorescence signal in AFB1-treated HepG2 cells. The ROS-associated fluorescence signal is expressed as a percentage of the control value. * $p < 0.05$; ** $p < 0.01$.

3.5. CGA Preserves Mitochondrial Membrane Potential and Modulates Apoptosis-Associated Transcripts

JC-1 staining showed a change in the red/green fluorescence distribution after AFB1 exposure, consistent with a reduction in mitochondrial membrane potential; the CGA-pretreated groups showed a less pronounced change in the representative images (Figure 9). These images were evaluated qualitatively, and a formal red/green fluorescence ratio was not calculated. In parallel, AFB1 increased *BAX* and *Caspase-3* mRNA expression and decreased *BCL-2* mRNA expression (Figure 10A–C). CGA partially attenuated these transcript changes, although the responses differed among genes and concentrations. In particular, the 25 μM CGA group did not show a greater reduction in *Caspase-3* mRNA than the 12.5 μM group.

3.6. CGA Modulates Intracellular Iron Levels and Ferroptosis-Associated Transcript Profiles

AFB1 exposure increased the measured intracellular Fe^{2+} and total iron levels (Figure 11). CGA pretreatment reduced both measurements relative to the AFB1-only group. AFB1 also increased *ACSL4*, *P53*, and *TXNIP* mRNA expression and decreased *Trx-1* and *GPX4* mRNA expression, whereas CGA partially shifted these transcript levels toward the control pattern (Figure 12). These results demonstrate changes in intracellular iron-associated measurements and selected ferroptosis-associated transcripts.

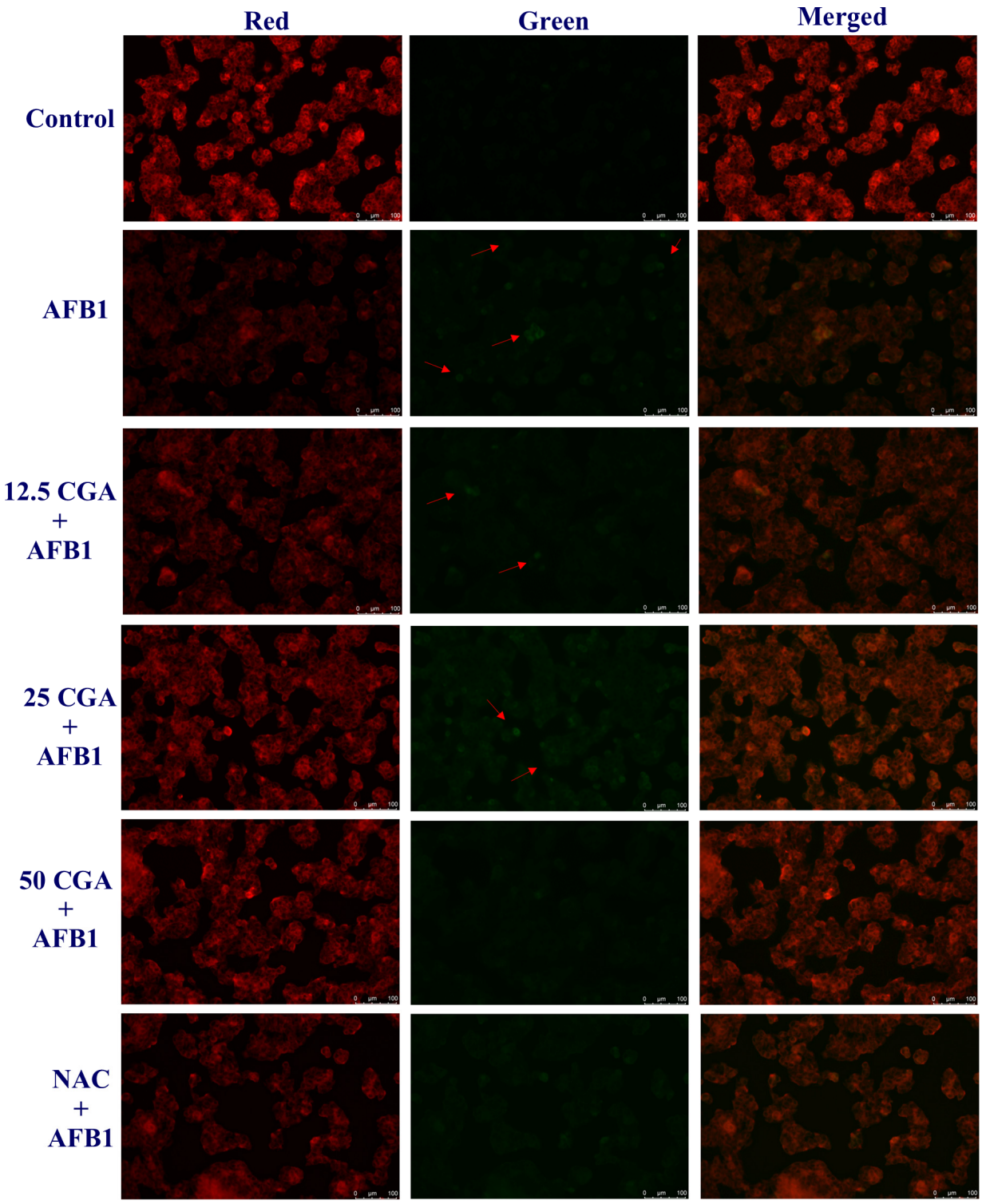


Figure 9. Representative JC-1 fluorescence images of HepG2 cells after the indicated treatments. Red fluorescence represents JC-1 aggregates associated with higher mitochondrial membrane potential, whereas green fluorescence represents JC-1 monomers associated with lower mitochondrial membrane potential. The images are presented qualitatively. The arrows indicate green fluorescence.

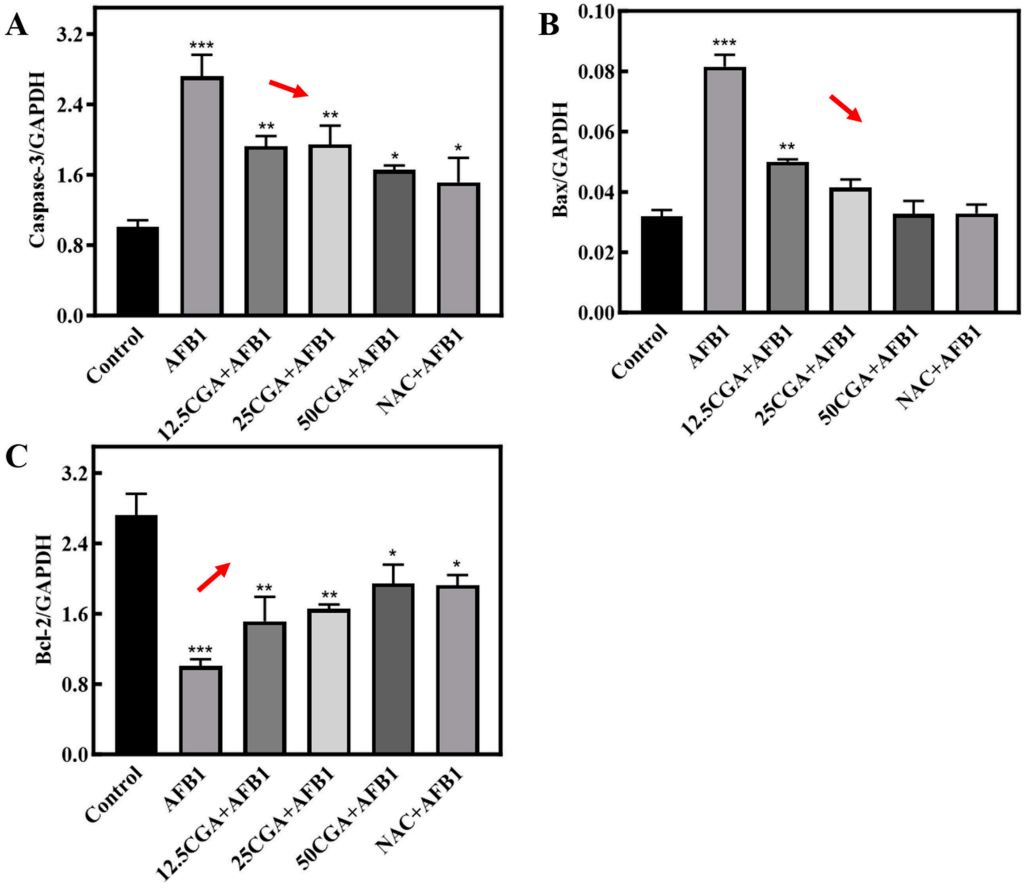


Figure 10. Relative mRNA expression of apoptosis-associated genes in AFB1-treated HepG2 cells: (**A**) *Caspase-3*, (**B**) *BAX*, and (**C**) *BCL-2*. Transcript abundance was normalized to *GAPDH* and calculated using the $2^{-\Delta Ct}$ method. * $p < 0.05$; ** $p < 0.01$; *** $p < 0.001$.

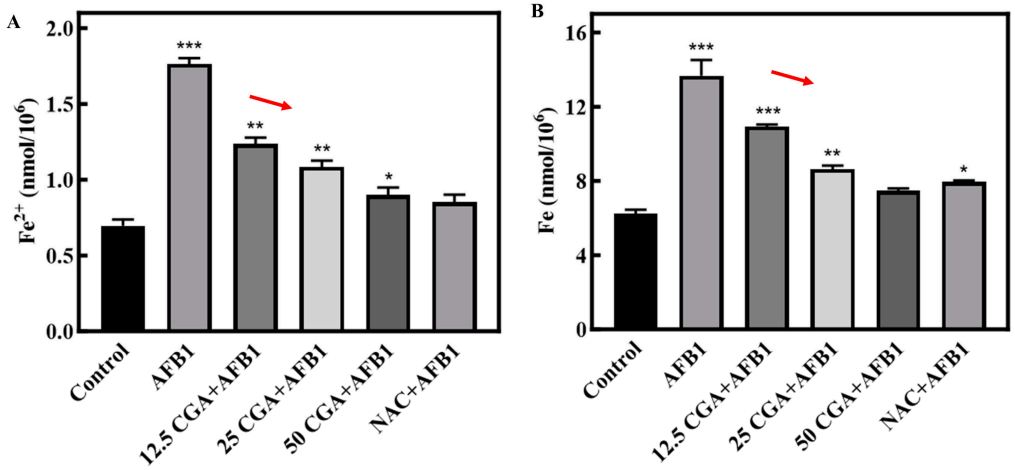


Figure 11. Effects of CGA pretreatment on intracellular (**A**) Fe^{2+} and (**B**) total iron levels in AFB1-treated HepG2 cells. Iron contents are expressed as nmol per 10^6 cells. * $p < 0.05$; ** $p < 0.01$; *** $p < 0.001$.

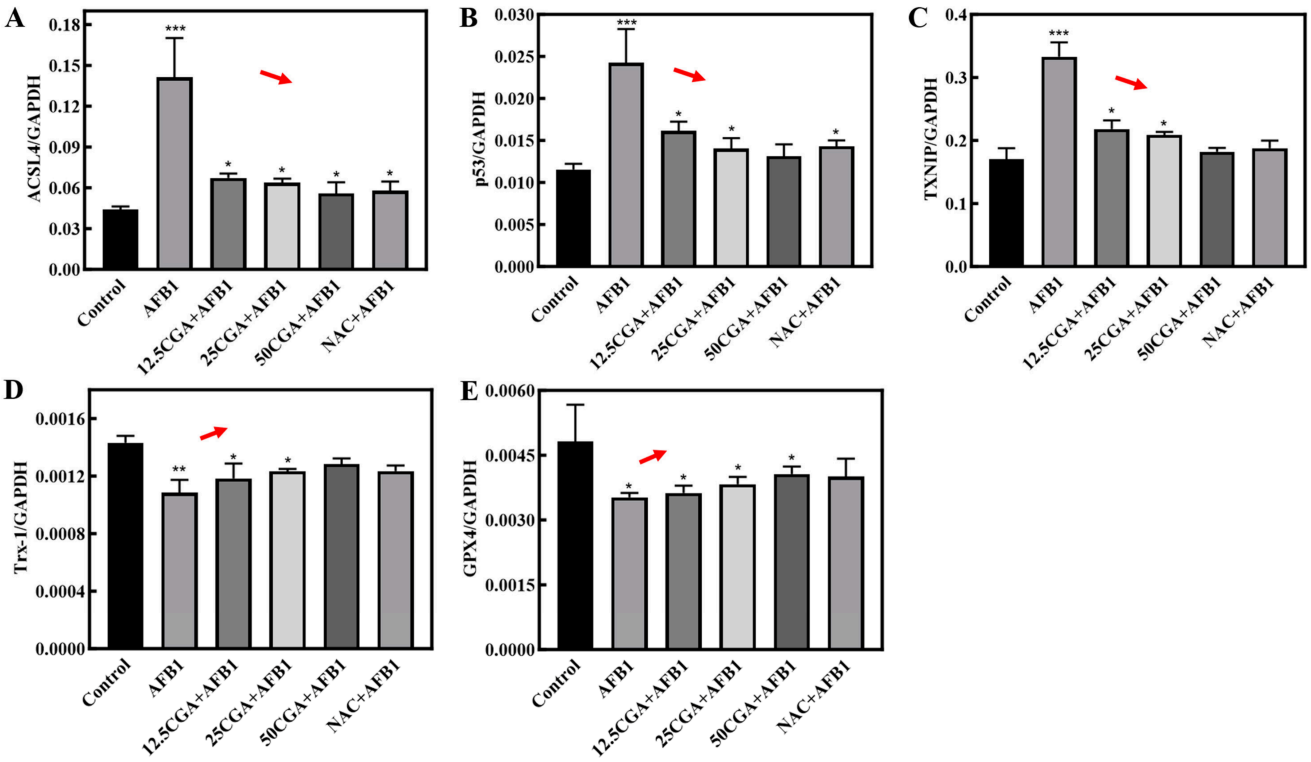


Figure 12. Relative mRNA expression of selected ferroptosis-associated genes in AFB1-treated HepG2 cells: (**A**) *ACSL4*, (**B**) *P53*, (**C**) *TXNIP*, (**D**) *Trx-1*, and (**E**) *GPX4*. Transcript abundance was normalized to *GAPDH* and calculated using the $2^{-\Delta Ct}$ method. * $p < 0.05$; ** $p < 0.01$; *** $p < 0.001$.

4. Discussion

The present study demonstrates that CGA pretreatment alleviates AFB1-induced injury in HepG2 cells across complementary cellular and biochemical endpoints. CGA improved cell viability and morphology, reduced extracellular LDH, ALT, and AST activities, increased GSH content and T-SOD activity, lowered ROS and LPO signals, and decreased intracellular Fe^{2+} and total iron levels. The convergence of these findings indicates that the protective effect of CGA is not confined to a single assay outcome but involves coordinated improvement in membrane integrity and cellular redox homeostasis. These results are consistent with previous reports of CGA-mediated protection against AFB1-induced liver injury [1,2] and extend this evidence by integrating mitochondrial, iron-related, and ferroptosis-associated transcript endpoints in a HepG2 model. NAC, included as a positive antioxidant reference, also improved several AFB1-associated endpoints. At several redox readouts, 50 μM CGA produced numerically favorable responses relative to NAC, supporting the potential of CGA as a protective phenolic compound in this model. Because the relative effects varied across endpoints, these comparisons indicate favorable activity for selected measures rather than universal superiority over NAC.

AFB1 exposure disrupted cellular redox balance, as reflected by decreased GSH content and T-SOD activity together with increased ROS, MDA, and LPO. CGA pretreatment shifted these indicators toward the control pattern, with clear improvements in GSH and T-SOD and reductions in ROS and LPO. Taken together, these changes support an antioxidant effect that contributes to the preservation of membrane integrity and cell viability. The increase in MDA was more modest than the change in LPO; this difference is reasonable because the assays measure distinct lipid-peroxidation-related outputs using different analytical principles. Mitochondrial responses provide a further dimension to the protective effect. AFB1 altered the JC-1 fluorescence distribution in a manner consistent with loss of mitochondrial

membrane potential, whereas CGA-pretreated cells showed a less pronounced shift. In parallel, CGA partially attenuated the AFB1-associated increases in *BAX* and *Caspase-3* mRNA and the decrease in *BCL-2* mRNA. These findings connect improved redox status and mitochondrial polarization with a more favorable apoptosis-associated transcriptional profile, consistent with reduced cellular stress. Similar changes in apoptosis-associated markers have been reported in AFB1-exposed models treated with natural compounds [44].

AFB1 exposure increased intracellular Fe^{2+} and total iron levels and altered the expression of ferroptosis-associated genes, including increased *ACSL4*, *P53*, and *TXNIP* mRNA and decreased *Trx-1* and *GPX4* mRNA. CGA pretreatment reduced both iron measurements and partially shifted these transcript levels toward the control pattern. Importantly, these changes occurred alongside improved GSH content and reduced LPO, linking iron-related responses with changes in lipid peroxidation and antioxidant defense. Because iron availability, lipid-peroxide accumulation, and glutathione-dependent antioxidant capacity are interconnected features of ferroptosis biology, the coordinated response observed here supports the conclusion that CGA attenuates ferroptosis-associated stress in AFB1-exposed HepG2 cells. This interpretation is consistent with previous reports connecting AFB1 hepatotoxicity with lipid peroxidation, ferritin autophagy, and *P53*-related signaling [27,28]. *P53* expression may also reflect a broader cellular stress response; therefore, its contribution is considered together with the iron, lipid-peroxidation, and other transcript measurements rather than as a stand-alone indicator. Overall, the findings identify iron- and lipid-peroxidation-related responses as an important component of the cytoprotective action of CGA. A flavonoid-rich Rhizoma Drynariae preparation has also been reported to mitigate AFB1-induced liver toxicity in chickens, although that in vivo model and its proposed microbiota–gut–liver mechanism differ from the present cell system [45].

The present study establishes a multi-endpoint cytoprotective effect of CGA and identifies redox, mitochondrial, and iron- and lipid-peroxidation-related responses associated with this protection. Several questions remain for further mechanistic investigation. In addition, biochemical endpoints were reported using different assay units and normalization bases, and altered cell number may have influenced measurements not normalized to cell number or protein. HepG2 cells also have lower hepatic metabolic competence than primary human hepatocytes, and AFB1 metabolism, CYP-mediated bioactivation, DNA adduct formation, and Nrf2/HO-1 signaling were outside the scope of the present experiments. Finally, the current work examined CGA pretreatment rather than intervention after injury had developed. These points define the scope of the present findings and provide clear directions for subsequent studies, including pathway-specific functional validation, protein-level analysis, appropriate cellular controls, and testing in metabolically competent hepatic models.

5. Conclusions

In conclusion, the present study demonstrates that the CGA preincubation/co-exposure regimen attenuates AFB1-associated cellular injury in HepG2 cells. The observed protective effects were accompanied by improvements in cellular redox status, less pronounced changes in JC-1 fluorescence, reduced intracellular Fe^{2+} and total iron levels, and partial modulation of selected apoptosis- and ferroptosis-associated transcripts. These findings suggest that the cytoprotective effects of CGA are associated with the regulation of oxidative stress, mitochondrial function, and iron- and lipid-peroxidation-related responses. Although further functional validation is required, the present findings provide experimental evidence supporting the potential role of CGA in mitigating AFB1-induced hepatocellular injury.

Author Contributions: D.J.: Writing—Original Draft, Formal Analysis, Methodology, Conceptualization, Funding Acquisition. M.Y.: Writing—Review & Editing, Formal Analysis. H.G.: Formal Analysis, Data Curation. L.L.: Formal Analysis, Supervision, Funding Acquisition. J.J.: Methodology, Data Curation. All authors have read and agreed to the published version of the manuscript.

Funding: This work was supported by the China Scholarship Council, China (No. 202307540001), National Key R&D Program of China (2024YFD1300803), Special Fund Project for Promoting High-quality Development of Marine and Fishery Industry of Fujian Province (FJHYF-L-2025-19), and Xiamen Key Science and Technology Plan Project of Future Industries (3502Z20254020). We appreciate those who helped directly and indirectly with this work.

Institutional Review Board Statement: Not applicable.

Informed Consent Statement: Not applicable.

Data Availability Statement: The original contributions presented in this study are included in the article. Further inquiries can be directed to the corresponding author.

Acknowledgments: During the preparation of this manuscript, the authors used DeepSeek V4 to improve the language and readability of the manuscript. The authors reviewed and edited the output as necessary and take full responsibility for the content of this publication.

Conflicts of Interest: The authors declare no conflicts of interest.

References

1. Cheng, K.; Niu, J.; Zhang, J.; Qiao, Y.; Dong, G.; Guo, R.; Zheng, X.; Song, Z.; Huang, J.; Wang, J.; et al. Hepatoprotective effects of chlorogenic acid on mice exposed to aflatoxin B1: Modulation of oxidative stress and inflammation. *Toxicon* **2023**, *231*, 107177. [CrossRef]
2. Wang, Q.; Liu, T.; Koci, M.; Wang, Y.; Fu, Y.; Ma, M.; Ma, Q.; Zhao, L. Chlorogenic Acid Alleviated AFB1-Induced Hepatotoxicity by Regulating Mitochondrial Function, Activating Nrf2/HO-1, and Inhibiting Noncanonical NF-κB Signaling Pathway. *Antioxidants* **2023**, *12*, 2027. [CrossRef]
3. Ye, L.; Chen, H.; Tsim, K.W.K.; Shen, X.; Li, X.; Li, X.; Lei, H.; Liu, Y. Aflatoxin B1 Induces Inflammatory Liver Injury via Gut Microbiota in Mice. *J. Agric. Food Chem.* **2023**, *71*, 10787–10797. [CrossRef]
4. Moloi, T.P.; Ziqubu, K.; Mazibuko-Mbeje, S.E.; Mabaso, N.H.; Ndlovu, Z. Aflatoxin B1-induced hepatotoxicity through mitochondrial dysfunction, oxidative stress, and inflammation as central pathological mechanisms: A review of experimental evidence. *Toxicology* **2024**, *509*, 153983. [CrossRef]
5. Choi, H.; Garavito-Duarte, Y.; Gormley, A.R.; Kim, S.W. Aflatoxin B1: Challenges and Strategies for the Intestinal Barrier. *Toxins* **2025**, *17*, 43. [CrossRef]
6. Albadrani, G.M.; Altyar, A.E.; Kensara, O.A.; Haridy, M.A.M.; Zaazouee, M.S.; Elshanbary, A.A.; Sayed, A.A.; Abdel-Daim, M.M. Effects of alfa-lipoic acid and coenzyme Q10 treatment on AFB1-induced oxidative, inflammatory, and DNA damages in rats. *Toxicon* **2024**, *249*, 108083. [CrossRef]
7. Altyar, A.E.; Kensara, O.A.; Noreldin, A.E.; Albadrani, G.M.; El-Demerdash, F.M.; Sayed, A.A.; Piscopo, M.; Mohammedsaleh, Z.M.; Al-Ghadi, M.Q.; Ghaboura, N. *Spirulina platensis* ameliorates hepatic oxidative stress and DNA damage induced by aflatoxin B1 in rats. *Toxicon* **2024**, *237*, 107553. [CrossRef]
8. Hemmati, N.; Anoush, M.; Kiasari, B.A.; Torkamani, A. Targeting ferroptosis as a therapeutic strategy for hepatotoxicity. *Toxicol. Rep.* **2025**, *15*, 102137. [CrossRef]
9. Hino, K.; Nishina, S.; Yanatori, I. Ferroptosis: Biology and role in liver disease. *J. Gastroenterol.* **2025**, *60*, 1339–1361. [CrossRef]
10. He, Y.; Lin, Y.; Song, J.; Song, M.; Nie, X.; Sun, H.; Xu, C.; Han, Z.; Cai, J. From mechanisms to medicine: Ferroptosis as a therapeutic target in liver disorders. *Cell Commun. Signal.* **2025**, *23*, 125. [CrossRef]
11. Jaeschke, H.; Ramachandran, A. Ferroptosis and intrinsic drug-induced liver injury by acetaminophen and other drugs: A critical evaluation and historical perspective. *J. Clin. Transl. Hepatol.* **2024**, *12*, 1057–1066. [CrossRef]
12. Lu, Y.; Hu, J.; Chen, L.; Li, S.; Yuan, M.; Tian, X.; Cao, P.; Qiu, Z. Ferroptosis as an emerging therapeutic target in liver diseases. *Front. Pharmacol.* **2023**, *14*, 1196287. [CrossRef]
13. Zhao, S.; Guo, Y.; Yin, X. Autophagy, ferroptosis, apoptosis and pyroptosis in metabolic dysfunction-associated steatotic liver disease. *Front. Biosci.-Landmark* **2024**, *29*, 30. [CrossRef]
14. Naowarojna, N.; Wu, T.W.; Pan, Z.; Li, M.; Han, J.R.; Zou, Y. Dynamic regulation of ferroptosis by lipid metabolism. *Antioxid. Redox Signal.* **2023**, *39*, 59–78. [CrossRef]
15. Pope, L.E.; Dixon, S.J. Regulation of ferroptosis by lipid metabolism. *Trends Cell Biol.* **2023**, *33*, 1077–1087. [CrossRef]

16. Kim, J.W.; Lee, J.Y.; Oh, M.; Lee, E.W. An integrated view of lipid metabolism in ferroptosis revisited via lipidomic analysis. *Exp. Mol. Med.* **2023**, *55*, 1620–1631. [CrossRef]
17. Mortensen, M.S.; Ruiz, J.; Watts, J.L. Polyunsaturated fatty acids drive lipid peroxidation during ferroptosis. *Cells* **2023**, *12*, 804. [CrossRef]
18. Sun, D.; Wang, L.; Wu, Y.; Yu, Y.; Yao, Y.; Yang, H.; Hao, C. Lipid metabolism in ferroptosis: Mechanistic insights and therapeutic potential. *Front. Immunol.* **2025**, *16*, 1545339. [CrossRef]
19. Endale, H.T.; Tesfaye, W.; Mengstie, T.A. ROS induced lipid peroxidation and their role in ferroptosis. *Front. Cell Dev. Biol.* **2023**, *11*, 1226044. [CrossRef]
20. Merkel, M.; Goebel, B.; Boll, M.; Adhikari, A.; Maurer, V.; Steinhilber, D.; Culmsee, C. Mitochondrial reactive oxygen species formation determines ACSL4/LPCAT2-mediated ferroptosis. *Antioxidants* **2023**, *12*, 1590. [CrossRef]
21. Punziano, C.; Trombetti, S.; Cesaro, E.; Grosso, M.; Faraonio, R. Antioxidant systems as modulators of ferroptosis: Focus on transcription factors. *Antioxidants* **2024**, *13*, 298. [CrossRef]
22. Wang, B.; Wang, Y.; Zhang, J.; Hu, C.; Jiang, J.; Li, Y.; Peng, Z. ROS-induced lipid peroxidation modulates cell death outcome: Mechanisms behind apoptosis, autophagy, and ferroptosis. *Arch. Toxicol.* **2023**, *97*, 1439–1451. [CrossRef]
23. Zhu, Y.; Fujimaki, M.; Rubinsztein, D.C. Autophagy-dependent versus autophagy-independent ferroptosis. *Trends Cell Biol.* **2025**, *35*, 745–760. [CrossRef]
24. Yang, H.; Dai, B.; Chen, L.; Li, Y.; Jin, X.; Gao, C.; Han, L.; Bian, X. Iberverin downregulates GPX4 and SLC7A11 to induce ferroptotic cell death in hepatocellular carcinoma cells. *Biomolecules* **2024**, *14*, 1407. [CrossRef]
25. Liu, Y.; Lu, S.; Wu, L.L.; Yang, L.; Yang, L.; Wang, J. The diversified role of mitochondria in ferroptosis in cancer. *Cell Death Dis.* **2023**, *14*, 519. [CrossRef]
26. Philpott, C.C.; Protchenko, O.; Wang, Y.; Novoa-Aponte, L.; Leon-Torres, A.; Grounds, S.; Tietgens, A.J. Iron-tracking strategies: Chaperones capture iron in the cytosolic labile iron pool. *Front. Mol. Biosci.* **2023**, *10*, 1127690. [CrossRef]
27. Song, C.; Wang, Z.; Cao, J.; Dong, Y.; Chen, Y. Hesperetin alleviates aflatoxin B1 induced liver toxicity in mice: Modulating lipid peroxidation and ferritin autophagy. *Ecotoxicol. Environ. Saf.* **2024**, *284*, 116854. [CrossRef]
28. Zhang, H.J.; Luo, J.Z.; Lan, C.L.; Teng, X.; Ge, B.; Liu, J.Q.; Xie, H.X.; Yang, K.J.; Qin, C.J.; Zhou, X. Baicalin protects against hepatocyte injury caused by aflatoxin B1 via the TP53-related ferroptosis pathway. *Ecotoxicol. Environ. Saf.* **2024**, *281*, 116661. [CrossRef]
29. Fu, Y.; Zhou, X.; Wang, L.; Fan, W.; Gao, S.; Zhang, D.; Ling, Z.; Zhang, Y.; Ma, L.; Bai, F. Salvianolic acid B attenuates liver fibrosis by targeting Ecm1 and inhibiting hepatocyte ferroptosis. *Redox Biol.* **2024**, *69*, 103029. [CrossRef]
30. Zhang, H.; Shi, H.; Li, X.; Zhou, S.; Song, X.; Ma, N.; Meng, M.; Chang, G.; Shen, X. Quercetin alleviates LPS/iE-DAP-induced liver injury by suppressing ferroptosis via regulating ferritinophagy and intracellular iron efflux. *Redox Biol.* **2025**, *81*, 103557. [CrossRef]
31. Chen, J.; Mu, M.; Lai, X.; Liu, C.; Luo, Y.; He, J.; Yu, B.; Wang, Q.; Wang, H.; Chen, D. Theaflavins attenuate iron overload-induced liver oxidative injury by inhibiting hepatocyte ferroptosis. *Int. J. Biol. Sci.* **2025**, *21*, 3030–3044. [CrossRef]
32. Ren, J.; Li, L.; Wen, R.; Yin, B.; Zhang, Y.; Wang, Z.; Zhu, S.; Pei, H.; Zhang, Z.; Sun, X. Sesamin alleviates ferroptosis in perfluorooctanesulfonate-induced liver injury by targeting Foxo1. *J. Agric. Food Chem.* **2025**, *73*, 15333–15345. [CrossRef]
33. Nguyen, V.; Taine, E.G.; Meng, D.; Cui, T.; Tan, W. Chlorogenic acid: A systematic review on the biological functions, mechanistic actions, and therapeutic potentials. *Nutrients* **2024**, *16*, 924. [CrossRef]
34. Zalewska, K.; Kulawik, M.; Gierszewska, J.; Gramala, Z.; Kalus, O.; Karpiński, M.; Maćkowiak, J.; Staniewski, A.; Szymańska, Z.; Zalewska, B. Chlorogenic acid's role in metabolic health: Mechanisms and therapeutic potential. *Nutrients* **2025**, *17*, 3303. [CrossRef]
35. Han, Z.; Batudeligen; Chen, H.; Narisu; Anda; Xu, Y.; Xue, L. Luteolin attenuates CCl4-induced hepatic injury by inhibiting ferroptosis via SLC7A11. *BMC Complement. Med. Ther.* **2024**, *24*, 193. [CrossRef]
36. Liu, Y.; Zhao, J.; Cong, W.; Liu, T.; Sha, K. Alpinetin pretreatment prevents lipopolysaccharide/D-galactosamine-induced acute liver injury in mice by inhibiting ferroptosis via the Nrf2/SLC7A11/GPX4 pathway. *Sci. Rep.* **2025**, *15*, 40065, Correction in *Sci. Rep.* **2026**, *16*, 5740.. [CrossRef]
37. Su, Y.; Zeng, Y.; Zhou, M.; Liao, M.; Qin, P.; Wu, R.; Han, J.; Liang, X.; Wang, Z.; Jiang, J. Natural polyphenol-mediated inhibition of ferroptosis alleviates oxidative damage and inflammation in acute liver injury. *Biomater. Res.* **2025**, *29*, 0167. [CrossRef]
38. Huang, W.; Chen, H.; He, Q.; Xie, W.; Peng, Z.; Ma, Q.; Huang, Q.; Chen, Z.; Liu, Y. Nobiletin protects against ferroptosis to alleviate sepsis-associated acute liver injury by modulating the gut microbiota. *Food Funct.* **2023**, *14*, 7692–7704. [CrossRef]
39. Fan, X.; Wang, X.; Hui, Y.; Zhao, T.; Mao, L.; Cui, B.; Zhong, W.; Sun, C. Genipin protects against acute liver injury by abrogating ferroptosis via modification of GPX4 and ALOX15-launched lipid peroxidation in mice. *Apoptosis* **2023**, *28*, 1469–1483. [CrossRef]
40. Guo, Y.; Chen, H.; Sun, J.; Zhang, J.; Yin, Y. Maresin1 inhibits ferroptosis via the Nrf2/SLC7A11/GPX4 pathway to protect against sepsis-induced acute liver injury. *J. Inflamm. Res.* **2024**, *17*, 11041–11053. [CrossRef]

41. Ye, Q.; Jiang, Y.; Wu, D.; Cai, J.; Jiang, Z.; Zhou, Z.; Liu, L.; Ling, Q.; Wang, Q.; Zhao, G. Atractylodin alleviates nonalcoholic fatty liver disease by regulating Nrf2-mediated ferroptosis. *Heliyon* **2023**, *9*, e18321. [CrossRef]
42. Wu, Z.; Zhu, Y.; Liu, W.; Balasubramanian, B.; Xu, X.; Yao, J.; Lei, X. Ferroptosis in liver disease: Natural active compounds and therapeutic implications. *Antioxidants* **2024**, *13*, 352. [CrossRef]
43. Liang, Y.; Qiu, S.; Zou, Y.; Luo, L. Targeting ferroptosis with natural products in liver injury: New insights from molecular mechanisms to targeted therapies. *Phytomedicine* **2024**, *122*, 155134. [CrossRef]
44. Rajput, S.A.; Shaukat, A.; Wu, K.; Rajput, I.R.; Baloch, D.M.; Akhtar, R.W.; Raza, M.A.; Najda, A.; Papliński, R.; Albrakati, A. Luteolin alleviates Aflatoxin B1-induced apoptosis and oxidative stress in the liver of mice through activation of Nrf2 signaling pathway. *Antioxidants* **2021**, *10*, 1268. [CrossRef]
45. Huang, S.; Lin, L.; Wang, S.; Ding, W.; Zhang, C.; Shaukat, A.; Xu, B.; Yue, K.; Zhang, C.; Liu, F. Total flavonoids of *Rhizoma Drynariae* mitigates aflatoxin B1-induced liver toxicity in chickens via microbiota-gut-liver axis interaction mechanisms. *Antioxidants* **2023**, *12*, 819. [CrossRef]

Disclaimer/Publisher's Note: The statements, opinions and data contained in all publications are solely those of the individual author(s) and contributor(s) and not of MDPI and/or the editor(s). MDPI and/or the editor(s) disclaim responsibility for any injury to people or property resulting from any ideas, methods, instructions or products referred to in the content.